

15. Jenny, A. & Keller, W. Cloning of cDNAs encoding the 160kDa subunit of the bovine cleavage and polyadenylation specificity factor. *Nucleic Acids Res.* **23**, 2629–2635 (1995).

16. Yoshimura, S. *et al.* Expression of *Xa1*, a bacterial blight-resistance gene in rice, is induced by bacterial inoculation. *Proc. Natl Acad. Sci. USA* **95**, 1663–1668 (1998).

17. Dong, F. *et al.* Rice (*Oryza sativa*) centromeric regions consist of complex DNA. *Proc. Natl Acad. Sci. USA* **95**, 8135–8140 (1998).

18. Oka, H. I. in *Rice Biotechnology* (eds Khush, G. S. & Toenniessen, G. H.) 55–80 (CAB International, Oxon, 1991).

19. Khush, G. S. Origin, dispersal, cultivation and variation of rice. *Plant Mol. Biol.* **35**, 25–34 (1997).

20. Yu, J. *et al.* A draft sequence of the rice genome (*Oryza sativa* L. ssp. *indica*). *Science* **296**, 79–92 (2002).

21. Goff, S. A. *et al.* A draft sequence of the rice genome (*Oryza sativa* L. ssp. *japonica*). *Science* **296**, 92–100 (2002).

22. Huang, X., Adams, M. D., Zhou, H. & Kerlavage, A. R. A tool for analyzing and annotating genomic sequences. *Genomics* **46**, 37–45 (1997).

23. Paterson, A. H. *et al.* Toward a unified genetic map of higher plants, transcending the monocot–dicot divergence. *Nature Genetics* **14**, 380–382 (1996).

24. Maugeness, S., Martinez, I., Godin, B., Perez, P. & Lescure, A. M. Structure of two maize phytase genes and their spatio-temporal expression during seedling development. *Plant Mol. Biol.* **39**, 503–514 (1999).

25. Knutzon, D. S. *et al.* Cloning of a coconut endosperm cDNA encoding a 1-acyl-sn-glycerol-3-phosphate acyltransferase that accepts medium-chain-length substrates. *Plant Physiol.* **109**, 999–1006 (1995).

26. Ewing, B. & Green, P. Base-calling of automated sequencer traces using Phred. II. Error probabilities. *Genome Res.* **8**, 186–194 (1998).

27. Gordon, D., Abajian, C. & Green, P. Consed. A graphical tool for sequence finishing. *Genome Res.* **8**, 195–202 (1998).

28. Burge, C. & Karlin, S. Prediction of complete gene structures in human genomic DNA. *J. Mol. Biol.* **268**, 78–94 (1997).

29. Altschul, S. F. *et al.* Gapped BLAST and PSI-BLAST: a new generation of protein database search programs. *Nucleic Acids Res.* **25**, 3389–3402 (1997).

30. Lowe, T. M. & Eddy, S. R. tRNAscan-SE: a program for improved detection of transfer RNA genes in genomic sequence. *Nucleic Acids Res.* **25**, 955–964 (1997).

Supplementary Information accompanies the paper on Nature's website (<http://www.nature.com/nature>).

Acknowledgements We thank T. Sasaki and the RGP for rice genetic and EST markers and a PAC genomic library of rice Nipponbare; R. Wing and the CUGI for providing BAC libraries of the Nipponbare variety; Monsanto for the rice working-draft sequence data; G. Barry and J. Liu for help; R. Buell and Q. Yuan for help with the annotation and analysis of chromosome 4 sequences; X. Huang and Z. Ning for help with using the *AAT* and the *ssaha* programs, respectively; members of the National Centre for Gene Research for assistance; Z. Xu, Z. Chen, G. Wang, Q. Ma and Q. Zhang for support; and X. Lin, X. Deng, Y. Li, L. Zhou, N. Zheng, X. Liu and members of the IRGSP for discussion. This work was supported by grants from the Ministry of Science and Technology of the People's Republic of China, Chinese Academy of Sciences, and the Shanghai Municipal Commission of Science and Technology.

Competing interests statement The authors declare that they have no competing financial interests.

Correspondence and requests for materials should be addressed to B.H. (e-mail: bhan@ncgr.ac.cn).

Multiplicative computation in a visual neuron sensitive to looming

Fabrizio Gabbiani*†, Holger G. Krapp*‡, Christof Koch* & Gilles Laurent*

* Division of Biology, California Institute of Technology, Pasadena, California 91125, USA

† Division of Neuroscience, Baylor College of Medicine, One Baylor Plaza, Houston, Texas 77030, USA

‡ Department of Zoology, University of Cambridge, Downing Street, Cambridge CB2 3EJ, UK

Multiplicative operations are important in sensory processing^{1–5}, but their biophysical implementation remains largely unknown^{5–10}. We investigated an identified neuron (the lobula giant movement detector, LGMD, of locusts) whose output firing rate in response to looming visual stimuli has been described by two models, one of which involves a multiplication. In this model, the LGMD multiplies postsynaptically two inputs (one excitatory, one inhibitory) that converge onto its dendritic tree^{11,12}; in the other model, inhibition is presynaptic to the

LGMD^{13,14}. By using selective activation and inactivation of pre- and postsynaptic inhibition, we show that postsynaptic inhibition has a predominant role, suggesting that multiplication is implemented within the neuron itself. Our pharmacological experiments and measurements of firing rate versus membrane potential also reveal that sodium channels act both to advance the response of the LGMD in time and to map membrane potential to firing rate in a nearly exponential manner. These results are consistent with an implementation of multiplication based on dendritic subtraction of two converging inputs encoded logarithmically, followed by exponentiation through active membrane conductances.

Several insect behaviours rely on tracking motion in depth: landing¹⁵, hovering flight¹⁶ and collision avoidance^{17–19}. These behaviours probably depend on different neural computations as animals actively move towards a target or, conversely, experience the approach of a moving threat. The LGMD (Fig. 1a) is an identified neuron located in the third visual neuropile of the locust optic lobe (lobula), and is part of a circuit thought to be involved in the generation of escape behaviours (Fig. 1b). It responds vigorously to solid objects approaching on a collision course with the animal^{17,18} (Fig. 1b, c). The LGMD fires throughout object approach with a rate that increases, peaks, and decreases as collision becomes imminent^{11,12}. Responses are typically brisker for small or fast-moving objects, leading to higher peak firing rates (f_{peak} ; Fig. 1d, top). But the timing of the peak firing rate is independent of the object's approach speed or size, and always follows with a fixed delay the time at which the object reaches a fixed threshold angular size, θ_{thres} , on the retina¹². This is seen by plotting the timing of the peak relative to collision (t_{peak}) as a function of the ratio $l/|v|$, where l is the object's half-size and $|v|$ its approach speed (Fig. 1b, d, bottom). The trigonometric relationship between l , v and the angular size, $\theta(t)$, subtended by the object during approach causes the points of such a graph to fall on a straight line if t_{peak} occurs with a fixed delay, δ , relative to θ_{thres} (refs 11, 12). The slope, α , of this straight line is related to θ_{thres} (ref. 12) and its y intercept equals δ . Such a linear relation is indeed observed experimentally^{11,12} (Fig. 1d, bottom; $\theta_{\text{thres}} = 17^\circ$, $\delta = 25$ ms). Thus for the LGMD in this animal, the peak firing rate always occurred 25 ms after the object reached 17° in angular size, independent of v or l .

The peak firing rate of the LGMD was not the only parameter related to threshold angular size during object approach: the time, t_{thres} , at which the firing rate reached a given value, here arbitrarily set at 50 spikes s^{-1} (Fig. 1c triangle), also fell on a straight line ($n = 10$) as a function of $l/|v|$ (Fig. 1d, bottom), and therefore anticipated with a fixed delay (here 101 ms, Fig. 1d) the time at which the object's angular size reached a fixed value (10°). This implies that decoding the LGMD's output by detecting either the peak or an arbitrary threshold instantaneous firing rate ($>50 \text{ spikes s}^{-1}$) conveys a reliable indicator of angular size during looming. The delay between angular threshold and peak firing time is independent of body temperature, arousal level, contrast, variations in shape or texture of the approaching object and direction of approach^{12,20}. Thus, angular threshold might be the image-based retinal variable used to trigger escape responses in the face of an impending collision. Indeed, a leg flexion (presumably in preparation for an escape jump) has been shown to follow the peak LGMD firing rate with a fixed delay¹¹. Angular object size is also closely related to obstacle avoidance behaviours in tethered flying locusts¹⁹.

How then does the LGMD compute this angular threshold? The LGMD receives, onto a large dendritic fan, excitatory retinotopic inputs that convey, to a first approximation, the angular velocity, $\dot{\theta}(t)$ of the approaching object²¹ (field A, Fig. 1a and b, green; Supplementary Information). In addition, two dendritic fields arborize in distinct regions of the lobula and receive phasic non-retinotopic, feedforward inhibition related to object size, $\theta(t)$

(refs 11, 22; fields B and C, Fig. 1a and b, red). We therefore investigated phenomenological models based on combinations of angular velocity and size^{11,12} that could describe the responses of the LGMD to approaching objects. The firing rate of the LGMD was fitted with functions of $\dot{\theta}(t)$ and $\theta(t)$ using a fixed number of parameters. Additive combinations of motion-dependent excitation and size-dependent inhibition could not fit experimental firing rate profiles. By contrast, fits based on the multiplication of an excitatory angular velocity term by an inhibitory (negative) exponential of object size, $[\dot{\theta} \exp(-\alpha\theta)]$, accounted well for most of the response time-course over a wide range of $l/|v|$ values in 10 neurons (Fig. 1c, blue line; Supplementary Information equation (1)). Theoretical arguments¹² show that only this multiplicative combination of excitation and inhibition predicts the linear relationship between peak firing rate and $l/|v|$ observed experimentally (Fig. 1d, bottom). These results suggest that the LGMD multiplies its two types of synaptic inputs related to motion and size of an approaching object.

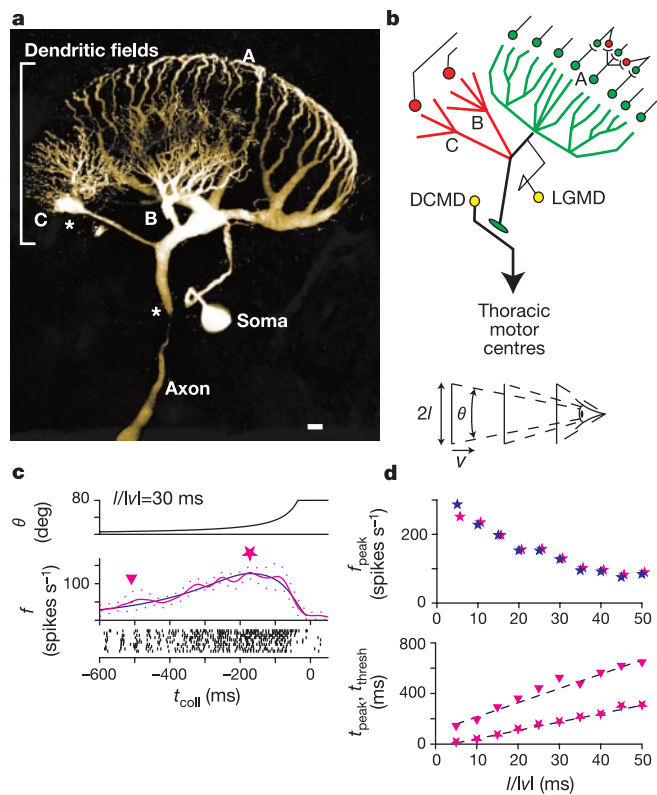


Figure 1 Properties of a neuronal circuit involved in locust escape behaviour and obstacle avoidance. **a**, The LGMD's large dendritic fan (A) arborizes in the lobula. Two additional dendritic arborizations (B, C) receive distinct synaptic inputs (asterisks represent dendritic and axonal recording sites of Figs 3 and 4; scale bar, 20 μm). **b**, top, fan A receives feedforward excitation (green), while B and C receive feedforward inhibition (red). Lateral inhibition (red) is presynaptic on the excitatory pathway (A). The LGMD synapses onto the DCMD, a neuron that relays spikes in a 1:1 manner to thoracic motor centres. Bottom, diagram illustrating the presentation of approaching squares (half-size, l ; velocity, $v < 0$; ref. 12). $\theta(t)$ depends only on $l/|v|$. **c**, Responses to approaching squares ($l/|v| = 30 \text{ ms}$). Top, angular size of the stimulus as a function of time relative to collision (t_{coll}). Middle, mean instantaneous firing rate \pm s.d. (magenta line and dots). Fit with multiplicative model in blue (Supplementary Information). Bottom, spike rasters (10 trials). Star, peak instantaneous firing rate. Triangle, threshold firing rate of 50 spikes s^{-1} . **d**, Top, peak instantaneous firing rate as a function of $l/|v|$ (maximal rate: $260 \pm 85 \text{ spikes s}^{-1}$, mean \pm s.d., 10 neurons). Blue stars, obtained from model fit as in **c**; mean correlation with $l/|v|$: -0.88 ± 0.19 (10 animals). Bottom, relation between peak (stars) or threshold (triangles) firing times relative to collision and $l/|v|$ is linear.

The excitatory motion-sensitive afferents to the LGMD are also subject to lateral inhibition mediated by a presynaptic network (Fig. 1b) that reduces responses to translating objects^{21,23}. Thus, an alternative model of the LGMD's responses to approaching objects has been proposed, where presynaptic and lateral—rather than postsynaptic and feedforward—inhibition competes with motion-dependent excitation during approach. In this model, feedforward postsynaptic inhibition intervenes only after object motion ceases^{13,14}. Numerical simulations showed that appropriately timed lateral inhibition could indeed play an important role in controlling excitation during object approach¹³. However, because object angular size, $\theta(t)$, depends nonlinearly on time during the approach, it is not clear whether experimental results obtained with translating objects carry over to approaching objects. Lateral inhibition is mediated by local interactions^{21,23} and as the object's angular speed increases during approach, it is expected to have decreasing influence because its speed of activation is limited by propagation time and synaptic delays¹³.

We set out to compare the contributions of feedforward (postsynaptic) and lateral (presynaptic) inhibition in controlling excitation during looming. We designed stimuli that preferentially activate either form of inhibition, and monitored their effect on the LGMD's firing profiles and peak firing time. Figure 2a illustrates one of eight experiments during which an approaching object (top)

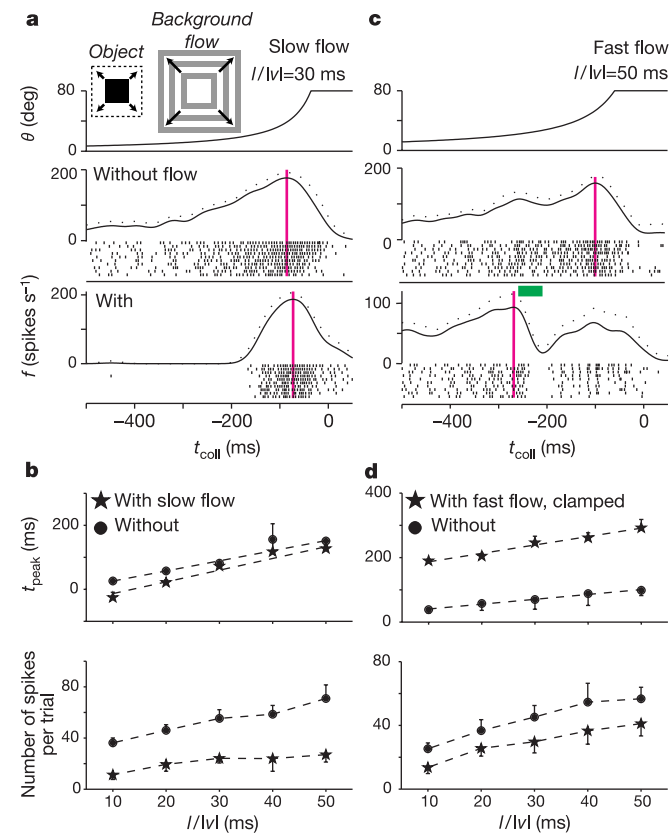


Figure 2 Effect of activating lateral or feedforward inhibition on peak firing time (magenta lines). **a**, Approaching stimulus (top) was presented either alone (middle) or in the presence of a pattern of white/grey stripes (bottom) slowly flowing outwards (inset). **b**, Peak firing time relative to collision with or without background pattern (top) and mean spike number (bottom) for each $l/|v|$ value (mean \pm s.d. 10 repetitions). **c**, Same as **a**, but the background pattern suddenly appeared (green horizontal bar) and moved outwards at a higher speed. **d**, Same as **b** for stimulus presented in **c**. In top panel, stars represent mean peak firing time in trials where it was clamped owing to background pattern motion. Data in **a**, **b** are from a different neuron than those in **c**, **d**.

was either shown alone (top raster) or superimposed on a patterned background (bottom raster) flowing slowly outwards from the centre of the screen (inset). Such slow-flowing stimuli predominantly activate lateral presynaptic inhibition without eliciting inhibitory postsynaptic potentials (IPSPs), that is, without invoking feedforward inhibition (Fig. 3; refs 21, 22). When shown in isolation, these stimuli did not elicit responses in the LGMD, except for 1–2 spikes at the onset of motion. When combined with a looming stimulus, the flowing background caused a significant reduction in the number of spikes fired by the LGMD at all $l/|v|$ values (Fig. 2b, bottom; $P < 0.0005$, rank-sum test). Yet, this reduction occurred exclusively early during the approach: as soon as the object exceeded $23.6^\circ \pm 12.2^\circ$ (8 animals, 5 $l/|v|$ values per animal), the LGMD's responses were virtually unaffected, except for a slight delay in peak firing time (Fig. 2a, b). Neither peak firing rate nor the number of spikes fired in a 100-ms window around the peak were statistically different under both conditions ($P > 0.1$, signed rank-sum test; $n = 8$).

These results contrast sharply with those obtained when the same patterned background appeared abruptly 200 ms before the end of looming (Fig. 2c, green bar) and flowed outwards for 50 ms at a high speed (10 animals; Methods). Such fast-flow stimuli effectively activate postsynaptic inhibition (refs 21, 22; Fig. 2d, bottom; $P < 0.05$, rank-sum test), a result confirmed by intracellular recordings (Fig. 3a). Activity of the LGMD ceased abruptly about 40 ms after fast-flow onset (Fig. 2c, bottom rasters). More

importantly, in 70% of approaches (for 10 animals) the time of peak firing was closely related to the time of fast-flow onset (Fig. 2d, top). Hence, for all values of $l/|v|$ tested, lateral inhibition could not antagonize excitation when the approaching stimulus was closest to collision ($\theta > 23.6^\circ$; Fig. 2a), whereas postsynaptic inhibition was highly effective, even during periods of robust LGMD excitation (Fig. 2c). These results indicate that, as contact nears, postsynaptic inhibition of the LGMD becomes increasingly important in controlling its firing.

We further investigated the time course of inhibition during object approach using local injection of picrotoxin (PCTX), a blocker of chloride channels^{24,25} (Methods; $n = 10$). The drug was applied to dendritic fields B and C of the LGMD. Because lateral inhibition is thought to be mediated by muscarinic acetylcholine receptors in the lobula²³, this manipulation selectively inactivated postsynaptic inhibitory inputs to the LGMD. Figure 3 illustrates LGMD responses to approaching objects before (Fig. 3a) and after (Fig. 3b) PCTX application. Block of postsynaptic inhibition during object approach increased response strength (Fig. 3c, left; $P < 0.008$, rank-sum test; $n = 10$) and peak instantaneous firing rate (Fig. 3c, right; $P < 0.008$, rank-sum test; $n = 10$) and prolonged the responses. To estimate the time at which postsynaptic inhibition started to control excitation significantly, we computed the angle subtended by the stimulus when the mean instantaneous firing rates in control and PCTX started to differ ($P > 0.05$, t -test).

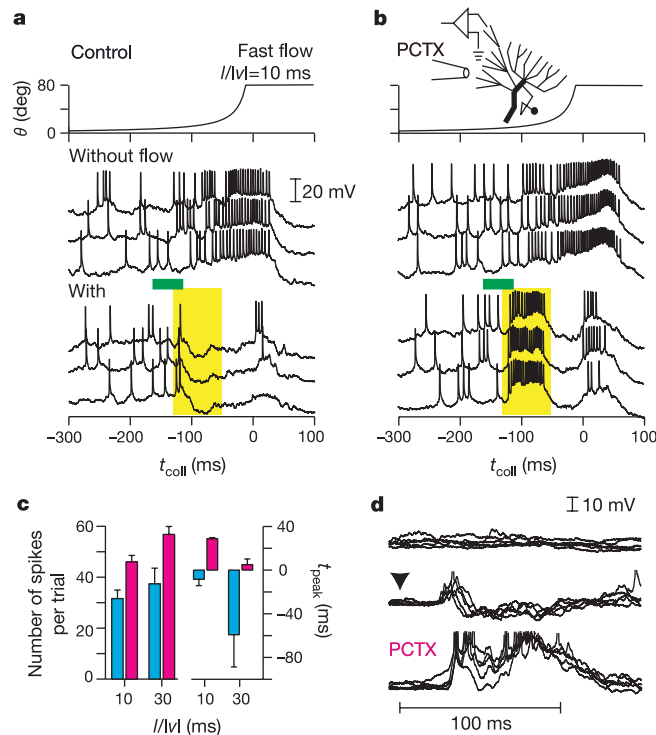


Figure 3 Effect of picrotoxin (PCTX) on the LGMD's responses to approaching stimuli. **a**, Middle 3 intracellular traces illustrate responses to an approaching stimulus (top, dendritic recording; **b**, schematic inset). Bottom 3 traces are responses to the same stimulus with the fast flow (green bar). Note the IPSPs (yellow). **b**, Same protocol after PCTX application (inset). The bottom 3 traces reveal excitation at the time when inhibition was previously present (yellow). **c**, Mean number of spikes (left) and mean peak firing time (right) before (blue) and after (red) PCTX application at two values of $l/|v|$ (\pm s.d., 5 repetitions). **d**, Presentation of the fast flow alone (arrow head, middle traces) elicits EPSPs followed by long-lasting IPSPs. In PCTX, IPSPs are replaced by EPSPs that elicit bursts of spikes (truncated). Top, responses to background alone. Data in **d** are from a different neuron than those in **a–c**.

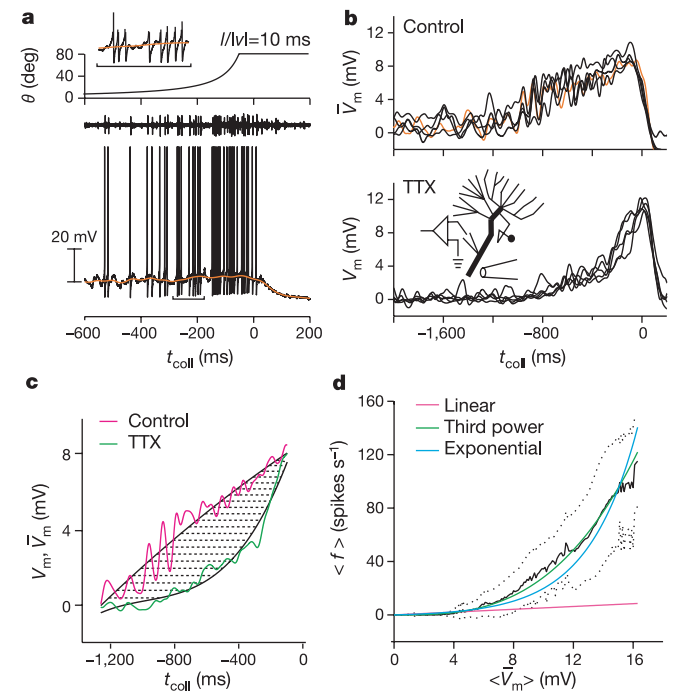


Figure 4 Transformation between membrane potential (V_m) and firing rate at the spike initiation zone. **a**, Approaching stimulus (top), recordings from the DCMD (middle, extracellular) and from the LGMD (bottom, intracellular) close to its spike initiation zone (inset). Orange trace is membrane potential after median filtering (\bar{V}_m). Inset, bracketed portion of V_m and (\bar{V}_m) expanded 3 times. **b**, Top panel presents median filtered membrane potential (orange line is same trace as in **a**; 5 repetitions). Bottom 5 traces were recorded after TTX application to the axon (inset). **c**, Mean traces in control and TTX (from **b**) were fitted with a third-order polynomial (black) and used to compute the mean temporal difference (352 ms) in membrane potential over the response rising phase. **d**, Fit of mean instantaneous firing rate, $\langle f \rangle$, as a function of mean, median filtered membrane potential (mean \pm s.d.; solid and dotted black lines) with linear, third-power and exponential models.

The average angle was $23.3^\circ \pm 19^\circ$ (mean \pm s.d., 10 animals and 4 $l/|v|$ protocols per animal), that is, similar to that beyond which lateral inhibition normally loses its influence on the LGMD's responses to an approaching object (Fig. 2a). From then on, the difference between instantaneous firing rate in control and PCTX steadily increased to reach 191% at the peak, consistent with inhibition depending on object size¹¹.

We then presented the approaching object in conjunction with the transient, fast outward flow shown in Fig. 2. Large IPSPs were seen in controls (Fig. 3a, yellow), consistent with previous results (Fig. 2c). Following PCTX injection, a strong excitatory response of duration similar to the presentation of the fast outward flow was revealed (Fig. 3b, yellow). Thus, the fast outward-flowing pattern normally activates concurrent excitation and inhibition, with inhibition rapidly dominating. To confirm this hypothesis we presented the transient fast outward-flow stimulus without approaching object, again in the absence and presence of PCTX (Fig. 3c; $n = 4$). In controls, an excitatory postsynaptic potential (EPSP) arose shortly after the onset of the flow stimulus (arrowhead), before being curtailed by a long-lasting IPSP. After PCTX injection, the same stimulus caused a strong and long-lasting excitation (Fig. 3d). We conclude that postsynaptic inhibition, presumably mediated by GABA_A synapses^{23,24}, potently controls the competing postsynaptic excitation.

Taken together, these results favour a scheme based on the control of excitation by postsynaptic rather than presynaptic inhibition during object approach. Furthermore, they show that the onset of postsynaptic inhibition is tightly matched to the fading of presynaptic inhibition. Under these conditions, a plausible model for the biophysical implementation of the multiplication of angular velocity (θ) and angular size ($\exp(-\alpha\theta)$) components could be by way of a postsynaptic subtraction of their logarithms²⁶, followed by exponentiation^{11,12}. This amounts to implementing $a \times (1/b)$ as $\exp(\log a - \log b)$, a technique commonly used in analogue integrated circuits²⁷. Because our phenomenological fits of the LGMD's responses characterize its firing rate as a function of $\theta \exp(-\alpha\theta)$, the exponentiation of $\log \theta - \alpha\theta$ could occur as the membrane potential is converted into spike output at the initiation zone by active membrane conductances. We tested this directly by characterizing the mapping between the intracellular membrane potential close to the spike initiation zone and firing frequency. Because the LGMD is a large neuron, intracellular recordings can be made either in its dendritic fields or in the axon, close to the initiation zone. The site of impalement is determined by the position of the recording electrode, and can be verified after staining the cell and from the action potential waveform at the recording site (dendritic, Fig. 3a, b; axonal, Fig. 4a, b).

We first determined whether voltage-dependent sodium channels in (or close to) the axon participate in any other way than in converting membrane potential into instantaneous firing rate. To this end, we recorded the axonal, intracellular membrane potential (V_m) in response to approaching objects before and after local injection of the sodium channel blocker tetrodotoxin (TTX) proximal to the recording site (Fig. 4b, inset). Drug ejection was monitored by adding a dye to the ejected solution (Methods). This pharmacological manipulation abolished firing responses while leaving peak depolarizing synaptic potentials unaffected (Fig. 4b). In contrast, injections of TTX in the second optic chiasm onto presynaptic excitatory afferents to the LGMD abolished all membrane depolarizations (not shown). The control membrane potential (\bar{V}_m ; in absence of TTX, Fig. 4b) was extracted by median filtering (Fig. 4a, inset, and 4b, orange lines; Methods). Comparison of TTX and control membrane potential traces revealed a considerable temporal shift (Fig. 4b), which we quantified by computing the average time difference between identical membrane potentials observed in the two conditions (average of the horizontal dotted lines' length in Fig. 4c). TTX-sensitive sodium conductances

advanced the response of the LGMD by 180 ± 110 ms (7 animals, 4 $l/|v|$ values per animal). Thus, TTX-sensitive conductances at or close to the spike initiation zone do not only serve to generate action potentials. They also normally accelerate the depolarization of the membrane potential during object approach.

Second, we measured the nonlinear transformation²⁸ between average postsynaptic potential at the axon (without pharmacological agents, after median filtering to remove spikes) and instantaneous firing rate. This nonlinear relationship is plotted in Fig. 4d for the experiment of Fig. 4a, b, averaged over different values of the looming stimulus parameter $l/|v|$. In this case, a third-order power law best described the transformation of membrane potential to firing rate (Fig. 4d). The same analysis was performed with 10 LGMD neurons, each from a different animal (Supplementary Table 1). In 7 out of 10 neurons (for example, Fig. 4d), a third-order power law best described the data. In one animal, no single-parameter model provided a good fit. In another, a sixth-order nonlinearity even closer to exponential than third order was required. In the last, exponential and third-power models could not be distinguished statistically.

Our experimental data suggest that two transformations occur between the LGMD membrane potential and firing rate during object approach. First is a temporal shift of the membrane potential time-course, resulting in a phase-advance of the spiking response (Fig. 4c). Because this shift represents a large fraction of the approach duration (>150 ms on average), it significantly amplifies motion-sensitive excitation. Together with the effective angular ranges of lateral and feedforward inhibition (Figs 2 and 3), this information places new constraints on the activation dynamics of presynaptic afferents to the LGMD during object approach. The second transformation is a nonlinear, expansive mapping of membrane potential into firing rate. Within the range of membrane potentials observed at the spike initiation zone, this transformation is best fitted by a third power that is remarkably close, but not identical, to an exponentiation (Fig. 4d). This suggests that either multiplication is only approximately implemented by a log-exp transform, or, alternatively, that part of the exponentiation occurs upstream of the spike initiation zone. Both transformations rely, at least in part, on TTX-sensitive channels.

In conclusion, we propose that the phenomenological fit between spatiotemporal features of approaching objects and the LGMD's firing rate—a product of two terms—represents the output of a dendritic and axonal implementation of multiplication by way of a log-exp transformation. We have suggested^{11,12} that multiplication could be carried out by the exponentiation of a sum of two postsynaptic currents or potentials: a positive excitatory one, representing the logarithm of angular velocity²⁶ and a negative one, representing angular size. We have shown here that the influence of angular velocity is excitatory and postsynaptic, and that the influence of angular size is inhibitory and postsynaptic. These results imply that multiplication occurs within LGMD itself, rather than presynaptically. Because the resulting axonal membrane potential maps onto output firing rate by way of an expansive nonlinearity close to an exponential, our experimental data are consistent with an approximate implementation by a log-exp transformation.

Multiplicative interactions between distinct sensory or extra-sensory variables have been reported in other preparations^{1–5}, although it has proved difficult either to identify the specific neurons responsible for these computations, or to map different sensory inputs onto distinct synaptic contributions to a single neuron. Thus the question of whether single neurons can implement multiplication remained largely open. Although several aspects of this computation remain to be characterized—in particular, the exact temporal dependence of feedforward excitation and inhibition on speed and size during object approach and their integration within the LGMD's dendritic tree—our results suggest

that the biophysical underpinning of such a nonlinear operation can be described mechanistically in a single neuron. □

Methods

Electrophysiology

Dissections and extracellular recordings from 45 descending contralateral movement detector (DCMD) neurons were as described in refs 12 and 20. We used extra-cellular recordings from the DCMD to monitor the spike activity of the LGMD because their spiking outputs match perfectly (Fig. 4a). Intracellular recordings from the LGMD ($n = 91$ animals) were obtained using glass microelectrodes filled with 2 M potassium acetate solution (30–80 MΩ). Typical intracellular recordings times were 40 min – 1 h. Stainings (Fig. 1a) were obtained by iontophoresis of Lucifer yellow (2% in aqueous solution). Local drug injections were performed using pulled and microforged glass micropipettes (final diameter, ~1 μm), backfilled with PCTX (5 mM) or TTX (1 μM) in aqueous solution and 0.5% (w/v) Fast green for visualization. Further technical details are available in Supplementary Information. Intracellular signals were amplified in bridge or DCC mode using an Axoclamp 2B (Axon Instruments) or SEL-10 (NPI) amplifier.

Visual stimulation

Visual stimulation procedures have been described previously^{12,20}. Briefly, black squares approaching perpendicular to the main body axis towards the eye (duration, 0.6–5.7 s) at various values of $l/|v|$ were presented in pseudo random order. Background flow stimuli consisted of alternating bright and grey (30% contrast) concentric rectangles moving outwards towards the screen boundaries at constant temporal frequency. For the slow-flow stimulus (Fig. 2a), the temporal frequency of light/dark transitions was set between 6 and 12 Hz. For the fast stimulus (Figs 2c, 3a, b, d), the temporal frequency was 50 Hz. Further details as well as procedures used to minimize habituation²⁹ of the responses are described in Supplementary information.

Data analysis

Data collection was performed using a PCI data acquisition card (UEI) and custom software²⁰. Sample rates were 10 kHz for extracellular, and 20 kHz for intracellular, recordings. Data analysis methods followed refs 12 and 20. Median filtering and fits of the LGMD/DCMD firing rate, $f(t)$, with various models are described in Supplementary Information. The relation between average membrane potential, $\langle V_m \rangle$, and firing rate, $\langle f \rangle$, (Fig. 4d) was obtained by averaging across trials membrane potential and instantaneous firing rate over 5-ms time windows and plotting one variable against the other. Linear ($\langle f \rangle = \alpha \langle V_m \rangle$), power law ($\langle f \rangle = \alpha \langle V_m \rangle^\beta$) and exponential ($\langle f \rangle = \exp(\alpha \langle V_m \rangle) - 1$) models depicted in Fig. 4d were fitted using maximum likelihood. Statistical tests followed ref. 30.

Received 1 August; accepted 20 September 2002; doi:10.1038/nature01190.

1. Reichardt, W. Autokorrelations-Auswertung als Funktionsprinzip des Zentralnervensystems. *Z. Naturforsch.* **12**, 448–457 (1957).
2. Barlow, H. B. & Levick, W. R. The mechanisms of directionally selective units in rabbit's retina. *J. Physiol. (Lond.)* **178**, 477–504 (1965).
3. McAdams, C. J. & Maunsell, J. H. R. Effects of attention on orientation-tuning functions of single neurons in macaque cortical area V4. *J. Neurosci.* **19**, 431–441 (1999).
4. Sun, H. & Frost, B. J. Computation of different optical variables of looming objects in pigeon nucleus rotundus neurons. *Nature Neurosci.* **1**, 296–303 (1998).
5. Pena, J. L. & Konishi, M. Auditory spatial receptive fields created by multiplication. *Science* **292**, 249–252 (2001).
6. Torre, V. & Poggio, T. A synaptic mechanism possibly underlying directional selectivity to motion. *Proc. R. Soc. Lond. B* **202**, 409–416 (1978).
7. Andersen, R. A., Essick, G. K. & Siegel, R. M. Encoding of spatial location by posterior parietal neurons. *Science* **23**, 456–458 (1985).
8. Yuste, R. & Tank, D. Dendritic integration in mammalian neurons, a century after Cajal. *Neuron* **16**, 701–716 (1996).
9. Koch, C. *Biophysics of Computation: Information Processing in Single Neurons* (Oxford Univ. Press, Oxford, 1998).
10. Chance, F. S., Abbott, L. F. & Reyes, A. D. Gain modulation from background synaptic input. *Neuron* **35**, 773–782 (2002).
11. Hatsopoulos, N., Gabbiani, F. & Laurent, G. Elementary computation of object approach by a wide-field visual neuron. *Science* **270**, 1000–1003 (1995).
12. Gabbiani, F., Krapp, H. G. & Laurent, G. Computation of object approach by a wide-field, motion-sensitive neuron. *J. Neurosci.* **19**, 1122–1141 (1999).
13. Rind, F. C. & Bramwell, D. I. Neural network based on the input organization of an identified neuron signaling impending collision. *J. Neurophysiol.* **75**, 967–985 (1996).
14. Rind, F. C. Intracellular characterization of neurons in the locust brain signaling impending collision. *J. Neurophysiol.* **75**, 986–995 (1996).
15. Wagner, H. Flow field variables trigger landing in flies. *Nature* **297**, 147–148 (1982).
16. Wickelmaier, M. & Strausfeld, N. J. Organization and significance of neurons that detect change of visual depth in the hawk moth *Manduca sexta*. *J. Comp. Neurol.* **424**, 356–376 (2000).
17. Schlotterer, G. R. Response of the locust descending movement detector neuron to rapidly approaching and withdrawing visual stimuli. *Can. J. Zool.* **55**, 1372–1376 (1977).
18. Rind, F. C. & Simmons, P. J. Orthopteran DCMD neuron: a reevaluation of responses to moving objects. I. Selective responses to approaching objects. *J. Neurophysiol.* **68**, 1654–1666 (1992).
19. Robertson, R. M. & Johnson, A. G. Retinal image size triggers obstacle avoidance in flying locusts. *Naturwissenschaften* **80**, 176–178 (1993).
20. Gabbiani, F., Mo, C. & Laurent, G. Invariance of angular threshold computation in a wide-field looming-sensitive neuron. *J. Neurosci.* **21**, 314–329 (2001).
21. O'Shea, M. & Rowell, C. H. F. Protection from habituation by lateral inhibition. *Nature* **254**, 53–55 (1975).

22. Rowell, C. H. F., O'Shea, M. & Williams, J. L. D. The neuronal basis of a sensory analyser, the acridid movement detector system. IV. The preference for small field stimuli. *J. Exp. Biol.* **68**, 157–185 (1977).
23. Rind, F. C. & Simmons, P. J. Local circuits for the computation of object approach by an identified visual neuron in the locust. *J. Comp. Neurol.* **395**, 405–415 (1998).
24. Rauh, J. J., Lummis, S. C. R. & Sattelle, D. B. Pharmacological and biochemical properties of insect GABA receptors. *Trends Pharmacol.* **11**, 325–329 (1990).
25. Warzecha, A. K., Egelhaaf, M. & Borst, A. Neural circuit tuning fly visual interneurons to motion of small objects. I. Dissection of the circuit by pharmacological and photoinactivation techniques. *J. Neurophysiol.* **69**, 329–339 (1993).
26. Zanker, J. M., Srinivasan, M. V. & Egelhaaf, M. Speed tuning in elementary motion detectors of the correlation type. *Biol. Cybern.* **80**, 109–116 (1999).
27. Mead, C. *Analog VLSI and Neural Systems* (Addison-Wesley, Boston, 1989).
28. Koch, C., Bernander, O. & Douglas, R. J. Do neurons have a voltage or a current threshold for action potential initiation? *J. Comput. Neurosci.* **2**, 63–82 (1995).
29. Rowell, C. H. F. in *Experimental Analysis of Insect Behavior* (ed. Browne, L. B.) 87–99 (Springer, New York, 1974).
30. Galant, A. R. *Non-linear Statistical Models* (Wiley & Sons, New York, 1987).

Supplementary Information accompanies the paper on Nature's website (<http://www.nature.com/nature>).

Acknowledgements We thank C. Mo for technical assistance with the experiments presented in Fig. 2, S. Potter for help with two-photon confocal microscopy, and J. Maunsell for comments. This work was supported by the Sloan Foundation, the National Institute of Mental Health (F.G., C.K.), the National Institute for Deafness and Communication Disorders (G.L.), the McKnight Foundation (G.L.) and the Center for Neuromorphic Engineering as part of the NSF Engineering Research Center programme. H.G.K. was supported by a travel grant of the Deutsche Forschungsgemeinschaft. F.G. is an Alfred P. Sloan research fellow.

Competing interests statement The authors declare that they have no competing financial interests.

Correspondence and requests for materials should be addressed to F.G. (e-mail: gabbiani@bcm.tmc.edu).

.....
Essential role for TIRAP in activation of the signalling cascade shared by TLR2 and TLR4

Masahiro Yamamoto*†, Shintaro Sato*†, Hiroaki Hemmi*†, Hideki Sanjo*†, Satoshi Uematsu*†, Tsuneyasu Kaisho*†‡, Katsuki Hoshino*†, Osamu Takeuchi*†, Masaya Kobayashi*†, Takashi Fujita§, Kiyoshi Takeda*† & Shizuo Akira*†

* Department of Host Defense, Research Institute for Microbial Diseases, Osaka University, and † Solution Oriented Research for Science and Technology, Japan Science and Technology Corporation, 3-1 Yamada-oka, Suita, Osaka 565-0871, Japan
 ‡ RIKEN Research Center for Allergy and Immunology, 1-7-22 Suehiro-cho, Tsurumi-ku, Yokohama, Kanagawa 230-0045, Japan
 § Department of Tumor Cell Biology, The Tokyo Metropolitan Institute of Medical Science, 3-18-22 Honkomagome, Bunkyo-ku, Tokyo 113-8613, Japan

.....
Signal transduction through Toll-like receptors (TLRs) originates from their intracellular Toll/interleukin-1 receptor (TIR) domain, which binds to MyD88, a common adaptor protein containing a TIR domain^{1–4}. Although cytokine production is completely abolished in MyD88-deficient mice, some responses to lipopolysaccharide (LPS), including the induction of interferon-inducible genes and the maturation of dendritic cells, are still observed^{5–7}. Another adaptor, TIRAP (also known as Mal), has been cloned as a molecule that specifically associates with TLR4 and thus may be responsible for the MyD88-independent response^{8,9}. Here we report that LPS-induced splenocyte proliferation and cytokine production are abolished in mice lacking TIRAP. As in MyD88-deficient mice, LPS activation of the nuclear factor NF-κB and mitogen-activated protein kinases